이학석사학위논문

East–west contrasting changes in Southern Indian Ocean Antarctic Bottom Water salinity over three decades

최근 30년 남빙양 인도양 구역 남극저층수의 대조적인 동서 염분 변화

2021년 8월

서울대학교 대학원

지구환경과학부

최 연

East–west contrasting changes in Southern Indian Ocean Antarctic Bottom Water salinity over three decades

최근 30년 남빙양 인도양 구역 남극저층수의
대조적인 동서 염분 변화

지도교수 남 성 현
이 논문을 이학석사 학위논문으로 제출함
2021 년 8 월

서울대학교 대학원
지구환경과학부
최 연

최 연의 이학석사 학위논문을 인준함
2021 년 8 월

위 원 장 _____ 조 양 기

부위원장 _____ 남 성 현

위 원 _____ 나 한 나

Abstract

East–west contrasting changes in Southern Indian Ocean Antarctic Bottom Water salinity over three decades

Yeon Choi

School of Earth and Environmental Sciences

The Graduate School

Seoul National University

Antarctic Bottom Water (AABW) characteristics, derived from multiple water sources with various properties, are significantly affected by and contribute to climate change. However, the in-depth causes of these changes are not well-understood. Here, I aimed to analyse the east–west contrasting pattern of changes in AABW characteristics in Southern Indian Ocean (SIO). Over the last three decades, AABW has become warmer and more saline in

the western SIO (WSIO) but warmer and fresher in the eastern SIO (ESIO), based on hydrographic observations since 1990. The warming and salinification of WSIO AABW are primarily explained by water source mixing ratios since the 1990s. In contrast, the warming and freshening of ESIO AABW are not explained by changes in the mixing ratio; instead, they are properties of the source waters during the same period. The east–west contrasting pattern of AABW salinity changes, in addition to overall warming, have imperative consequences in terms of poleward AABW transport and sea level rise within and beyond the SIO.

Keywords: Antarctic Bottom Water (AABW), Southern Ocean Indian Sector, Repeated hydrography data, simple Optimium Multiparameter analysis (OMP), Contrasting salinity changes, Global Warming

Student Number: 2019-20179

Contents

List of Tables

List of Figures

1. Introduction

Antarctic Bottom Water (AABW), generally referred to as seawater with a potential temperature (θ) less than 0 ^{o}C or neutral density (γ^{n}) greater than 28.27 kg m^{-3}, forms near the Antarctic continental margins (Orsi et al., 2002; Johnson et al., 2008; Jacobs, 2004; Orsi et al., 1999; Menezes et al., 2017). AABW ventilates the abyssal ocean, sequesters heat and carbon, and regulates the global overturning circulation and atmospheric carbon dioxide (Orsi et al., 1999; Menezes et al., 2017; Purkey and Johnson, 2013; Mahieu et al., 2020). There are four regions of AABW formation; slightly different properties of AABW have been identified among these regions (Orsi et al., 1999; Menezes et al., 2017; Rintoul, 2007; Ohshima et al., 2013; JAcobs and Giullivi, 2010; Williams et al., 2010; Kusahara et al., 2011b; Orsi, 2010; Talley et al., 2011) (Figure 1). In particular, the AABW properties in the Indian sector of Southern Ocean (Southern Indian Ocean; hereafter SIO) are determined by conditions in the formation regions with an abyssal circulation primarily constrained by bathymetry and major currents such as the eastward-flowing Antarctic Circumpolar Current (ACC) and westward-flowing Antarctic Slope Current near the Antarctic shelves (Jacobs, 2004;

Orsi, 2010; Talley et al., 2011; McCartney and Donohue, 2007; Meijers et al., 2010). AABW in the western SIO (WSIO) reflects properties of source waters such as Lower Circumpolar Deep Water (LCDW), Weddell Sea Deep Water (WSDW), and Cape Darnley Bottom Water (CDBW) Thomas et al., 2020; Aoki et al., 2020a). In contrast, AABW in the eastern SIO (ESIO) consists of LCDW, Adélie Land Bottom Water (ALBW), and Ross Sea Bottom Water (RSBW) (Figure 1, Table 1) (Aoki et al., 2020b; Strass et al., 2020). Anthropogenic greenhouse gas emissions have affected ocean circulation (Sallée, 2018; Levitus et al., 2005), through forcing pattern changes in, e.g., Southern Annular Mode (SAM) (Cai et al., 2005; Silvano et al., 2020), and consequently, have impacted the properties of AABW and its source waters (Purkey and Johnson, 2010; Purkey and Johnson, 2012; Lumpkin and Speer, 2007; van Wijk and Rintoul; 2014). Continued warming and freshening of AABW in the ESIO have been identified. Increases in θ at 0.02–0.08 ℃ decade^{-1} (Johnson et al., 2008; Menezes et al., 2017; Purkey and Johnson, 2013; Shimada et al., 2012) and decreases in practical salinity (S_P) of 0.002–0.012 decade^{-1} have been observed between the 1990s and 2000s (Purkey and Johnson, 2013). Significant warming (> 0.03^{o}C decade^{-1}) before 2000 (Sallée, 2018) and slight salinification (< 0.001 decade^{-1}) in the

WSIO (near 40°E) between the 1970s and 2010s have also been reported (Aoki et al., 2020a). However, despite few previous studies on changes in the AABW characteristics during recent decades, my understanding of their causes remains incomplete. Here, this study analysed an east–west contrasting salinity change (ΔS_P) in AABW (defined as $\theta < 0$°C and $\gamma^n > 28.27$ kg m^{-3}) in addition to overall warming ($\Delta\theta > 0$) in the WSIO and ESIO over the past three decades. My analysis demonstrates how the mixing ratio among and properties of source waters affect the AABW characteristics in terms of global ocean circulation under changing climate.

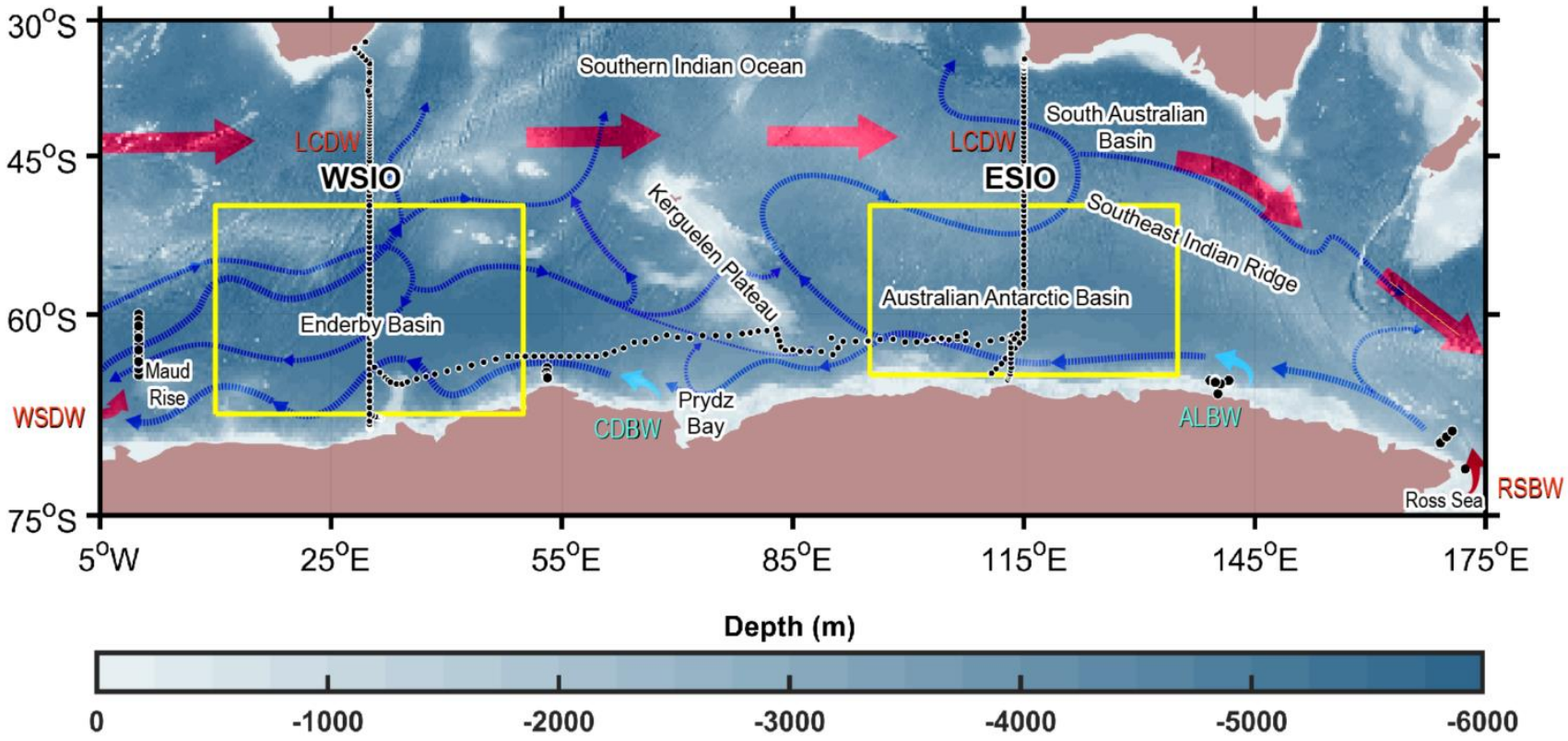

Figure 1. Schematic of the primary sources and paths of Antarctic Bottom Water (AABW) in Southern Indian Ocean (SIO), with ocean depth highlighted. Schematic pathways of AABW (blue dashed arrows) and Lower Circumpolar Deep

Water (LCDW; thick red arrows) based on previous work (Orsi et al,, 2002; Jacobs, 2004; Menezes et al., 2017; Mahieu et al., 2020; Rintoul, 2007; Ohshima et al., 2013; Orsi, 2010; Talley et al., 2011; McCartney and Donohue, 2007; Meijers et al., 2010; Thomas et al., 2020; Aoki et al., 2020a; Aoki et al., 2020b; Strass et al., 2020; van Wijk and Rintoul, 2014; Van Heuven et al., 2011; Vernet et al., 2019; Couldrey et al., 2013) are superimposed with ocean depth (shaded). Source water formation regions (Weddell Sea Deep Water, WSDW; Cape Darnley Bottom Water, CDBW; Adélie Land Bottom Water, ALBW; and Ross Sea Bottom Water, RSBW) are marked using solid arrows and labels (red for WSDW and RSBW, cyan for CDBW and ALBW). The black dots indicate locations of ship-based hydrographic data collection. Yellow boxes indicate satellite altimetry missions sites.

.

Table 1. Mean time difference (Δt, years), potential temperature (θ, ºC), practical salinity (S_P), and differences and trends (1990s to 2010s) of θ and S_P for observed (Case 1) and estimated (Case 2) Antarctic Bottom Water (AABW) and corresponding source waters in the western SIO (WSIO) and eastern SIO (ESIO). Confidence intervals (95%) are written after each value. Case 1 (Case 2) reproduced the AABW characteristics using time-varying (fixed) mixing ratios among and fixed (time-varying) properties of source waters.

Observation area	Water mass considered	Δt* (year)	θ (ºC)		Δθ (ºC)	Δθ/Δt (ºC decade^{-1})
			1990s	2010s	2010s minus 1990s	
WSIO	AABW (Observation)	24.5	-0.41 ± 0.01	-0.36 ± 0.01	0.05 ± 0.02	0.02 ± 0.01
	AABW (Case 1)		-0.45 ± 0.01	-0.35 ± 0.01	0.10 ± 0.02	0.04 ± 0.01
	AABW (Case 2)		-0.36 ± 0.01	-0.41 ± 0.01	-0.05 ± 0.02	-0.02 ± 0.01
	CDBW	20.0	-0.35 **	-0.43 ± 0.02	-0.08 ± 0.02	-0.04 ± 0.01
	WSDW	16.3	-0.68 ± 0.02	-0.70 ± 0.01	-0.02 ± 0.03	-0.01 ± 0.02
	LCDW	24.5	2.03 ± 0.21	2.06 ± 0.01	0.03 ± 0.22	0.01 ± 0.09
ESIO	AABW (Observation)	17.0	-0.18 ± 0.01	-0.13 ± 0.01	0.05 ± 0.02	0.03 ± 0.01
	AABW (Case 1)		-0.13 ± 0.01	-0.13 ± 0.01	0.00 ± 0.02	0.00 ± 0.01
	AABW (Case 2)		-0.23 ± 0.01	-0.16 ± 0.01	0.07 ± 0.02	0.04 ± 0.01
	RSBW	23.3	-0.72 **	-0.53 ± 0.05	0.19 ± 0.05	0.08 ± 0.03
	ALBW	19.3	-0.71 ± 0.08	-0.69 ± 0.08	0.02 ± 0.16	0.01 ± 0.08
	LCDW	17.0	1.76 **	1.76 **	0.00 **	0.00 **

Observation area	Water mass considered	Δt* (year)	S_P		ΔS_P	$\Delta S_P/\Delta t$ (decade^{-1})
			1990s	2010s	2010s minus 1990s	
WSIO	AABW (Observation)	24.5	34.660 ± 0.001	34.664 ± 0.001	0.004 ± 0.002	0.002 ± 0.001
	AABW (Case 1)		34.657 ± 0.001	34.664 ± 0.001	0.007 ± 0.002	0.003 ± 0.001

	AABW (Case 2)		34.663 ± 0.001	34.661 ± 0.001	-0.002 ± 0.002	-0.001 ± 0.001
	CDBW	20.0	34.659 **	34.650 ± 0.006	-0.009 ± 0.006	-0.005 ± 0.003
	WSDW	16.3	34.651 ± 0.002	34.659 ± 0.001	0.008 ± 0.003	0.005 ± 0.002
	LCDW	24.5	34.819 ± 0.024	34.826 ± 0.001	0.007 ± 0.025	0.003 ± 0.01
ESIO	AABW (Observation)	17.0	34.679 ± 0.001	34.673 ± 0.001	-0.006 ± 0.002	-0.004 ± 0.001
	AABW (Case 1)		34.672 ± 0.001	34.681 ± 0.001	0.009 ± 0.002	0.005 ± 0.001
	AABW (Case 2)		34.686 ± 0.001	34.668 ± 0.001	-0.018 ± 0.002	-0.011 ± 0.001
	RSBW	23.3	34.726 **	34.696 ± 0.027	-0.030 ± 0.027	-0.013 ± 0.014
	ALBW	19.3	34.636 ± 0.003	34.619 ± 0.001	-0.017 ± 0.004	-0.009 ± 0.002
	LCDW	17.0	34.754 **	34.751 **	-0.003 **	-0.002 **

* Time difference of two observation periods between the 2010s and 1990s, estimated after averaging the observation periods in each decade from the years listed in Table 2.

** Confidence interval is not available from one sample from a single cruise for the corresponding decade.

2. Data and method

AABW definition and data processing

All high-quality hydrographic Conductivity-Temperature-Depth (CTD) data used in this study were provided by the CLIVAR Carbon Hydrographic Data Office website (https://cchdo.ucsd.edu/). The CTD data meridionally observed along the observational lines in 1993, 1996, and 2019 in the WSIO and 1995 and 2012 in the ESIO were used to analyse AABW changes between the 1990s and 2010s (Table 2), and zonally observed along the observational lines in 1996 and 2013 were used to analyse geostrophic velocity changes between the 1990s and 2010s (Table 2). To facilitate comparison of the observed data with those of previous studies, in situ temperature and practical salinity (S_P) were used to convert potential temperature (θ), potential density reference pressure of 4,000 dbar (σ_4), and neutral density (γ^n) (Jackett and McDougall, 1997) through the formula in the Gibbson Seawater Toolbox v3.06 and (eos80_legacy_gamma_n) provided by the Thermodynamic Equation of Seawater 2010 (TEOS-10; http://www.teos-10.org/) and PreTEOS-10 (http://www.teos-10.org/preteos10_software/). Unnecessary noise was removed from the CTD data using a moving average over a 20-dbar interval and then linearly interpolated to

0.1° X 10-dbar intervals through scattered interpolant along the meridional lines 68°S and 28°S in the WSIO and ESIO. The CTD data collected near or closer to 10-dbar from the seafloor were removed based on the Smith-Sandwell bathymetry (Smith and Sandwell, 1997) with no extrapolation. Bathymetry data derived from a 1-arcminute global relief model (ETOPO1; http://www.ngdc.noaa.gov/mgg/global/global.html) were used to draw the map shown in Figure 1. To estimate the statistical significance of changes in AABW θ and S_P, 95% confidence interval from Student's *t*-test distribution was used, as given by $\bar{x} \pm t_{\alpha/2_v} \frac{s}{\sqrt{v}}$, where $\bar{x}$, s, v, and $t_{\alpha/2_v}$ represent the mean and standard deviation of the samples, effective degrees of freedom, and critical value of the *t* statistic of v, respectively (Menezes et al., 2017). A spatial decorrelation length scale of 160 km used in a previous study (Menezes et al., 2017) was applied to estimate the effective degrees of freedom. To estimate the θ and S_P differences in AABW between the 1990s and 2010s, the AABW domain was defined where $\gamma^n > 28.27$ kg m^{-3} and $\theta < 0$°C.

Estimation of sea level changes

Total sea level changes between 1990s and 2010s were estimated using satellite altimetry missions data provided by E.U. Copernicus Marine Service Information (CMEMS) (1990s; 1993-01-01 to 1999-12-31, 2010s; 2010-01-01 to 2019-12-31). The satellite observation areas were selected by the location 20 degrees away from the east and west of the meridional CTD line with latitude based on AABW distribution (Figure 1). To estimate steric sea level changes between 1990s and 2010s, Thermodynamic Equation of Seawater 2010 (TEOS-10) methods were used in this study. Non-steric sea level changes were calculated by subtracting the steric sea level changes of the entire water column measured by CTD data from the total sea level changes measured by satellite altimetry data.

Determination of source water properties

To reproduce the AABW characteristics, CTD data collected in the 1990s and 2010s along the observational lines listed in Table 2 were used. The endmembers of source waters were estimated from CTD data based on previous studies (Figure 3, Table 1) (Ohshima et al., 2013; Thomas et al., 2020; Aoki et al., 2020a; Aoki et al., 2020b; Strass et al., 2020). In the WSIO, endmembers of three source waters (WSDW, CDBW, LCDW) were determined by averaging θ and S_P over the following areas: $-0.7^oC < \theta < 0^oC$ within 60^o–65^oS and 0.5^oW–

0.5°E with a maximum depth > 2,500 dbar for WSDW, 64–70°S and 50–61°E with a maximum depth > 2,500 dbar for CDBW, and maximum salinity of 28.05 < γ^n < 28.27 kg m^{-3} for LCDW (Aoki et al., 2020a; Strass et al., 2020) (Table 1, Table 2). In the ESIO, endmembers of three source waters (RSBW, ALBW, and LCDW) were determined by averaging θ and S_P over the following areas: For RSBW, 69.2–78°S and 160–180°E with a maximum depth > 1,300 dbar, 65.4–68.2°S and 138–142°E with a maximum depth > 400 dbar for ALBW, and maximum salinity in 28.05 < γ^n < 28.27 kg m^{-3} for LCDW **(**Table 1, Table 2) (Ohshima et al., 2013; Thomas et al., 2020; Aoki et al., 2020b).

Table 2. Summary of ship-based hydrography data used in this study

Water of concern	Section	Period	Year	Mean year	Research Vessel	Cruise designator	Publication (if available)
AABW	WSIO	1990s	1993	1994.5	R/V Marion	35MFCIVA_1	Purkey and Johnson (2011)
			1996		R/V Marion	35MF103_1	Purkey and Johnson (2011)
		2010s	2019	2019.0	R/V Thomas G. Thompson	325020190403	
	ESIO	1990s	1995	1995.0	R/V Knorr	316N145_5	Purkey and Johnson (2011)
		2010s	2012	2012.0	R/V Aurora Australis	09AR20120105	Aoki et al (2020b)
	ZSIO*	1990s	1996	1996	R/V Nathaniel B. Palmer	320696_3	
		2010s	2013	2013	R/V Mirai	49NZ20130106	
Water of concern	**Section**	**Period**	**Year**	**Mean year**	**Research Vessel**	**Cruise designator**	**Publication (if available)**
LCDW	WSIO	1990s	1993	1994.5	R/V Marion	35MFCIVA_1	Purkey and Johnson (2011)
			1996		R/V Marion	35MF103_1	Purkey and Johnson (2011)
		2010s	2019	2019.0	R/V Thomas G. Thompson	325020190403	Purkey and Johnson (2011)
	ESIO	1990s	1995	1995.0	R/V Knorr	316N145_5	Purkey and Johnson (2011)
		2010s	2012	2012.0	R/V Aurora Australis	09AR20120105	Aoki et al (2020b)
CDBW	WSIO	1990s	1996	1996.0	R/V Nathaniel B. Palmer	320696_3	
		2010s	2013	2016.0	R/V Mirai	49NZ20130106	
			2019		R/V Mirai	49NZ20191229	
WSDW		1990s	1992	1995.7	R/V Polarstern	06AQANTX_4	Fahrbach et al. (2004)
			1996		RV Polarstern	06AQANTXIII_4	Fahrbach et al. (2004)
			1999		R/V Polarstern	06AQ199901_2	Fahrbach et al. (2004)
		2010s	2010	2012.0	R/V Polarstern	06AQ20101128	
			2014		R/V Polarstern	06AQ20141202	
ALBW	ESIO	1990s	1994	1995.3	R/V Aurora Australis	09AR9407_1	Aoki et al (2020b)
			1995		R/V Aurora Australis	09AR9404_1	Aoki et al (2020b)
			1996		R/V Aurora Australis	09AR9604_1	Aoki et al (2020b)
			1996		R/V Aurora Australis	09AR9601_1	
		2010s	2011	2014.5	R/V Aurora Australis	09AR20110104	Aoki et al (2020b)
			2018		R/V Investigator	096U20180111	Aoki et al (2020b)
RSBW		1990s	1992	1992.0	R/V Akademik Ioffe	90KDIOFFE6_1	Aoki et al (2020b)
		2010s	2011	2015.0	R/V Nathaniel B. Palmer	320620110219	Aoki et al (2020b)
			2017		R/V Nathaniel B. Palmer	320620170410	
			2018		R/V Nathaniel B. Palmer	320620180309	Aoki et al (2020b)

* ZSIO; Zonal sections of Southern Indian Ocean between 30°E and 110°E

Reproducing AABW temperature and salinity

Characteristics of AABW were reproduced through a simple Optimum Multiparameter analysis using two conservative source water tracers (θ and S_P) (Thomas et al., 2020).

$$x_1\theta_{\mathrm{WM1}} + x_2\theta_{\mathrm{WM2}} + x_3\theta_{\mathrm{WM3}} = \theta_{AABW} \quad (1)$$

$$x_1 S_{\mathrm{WM1}} + x_2 S_{\mathrm{WM2}} + x_3 S_{\mathrm{WM3}} = S_{AABW} \quad (2)$$

$$x_1 + x_2 + x_3 = 1 \quad (3)$$

Equations (1) to (3) represent heat, salt, and mass conservation, respectively. θ_{WM1} to θ_{WM3} and S_{WM1} to S_{WM3} denote the θ and S_P of source waters, determined from observations (Table 1), and x_1, x_2, and x_3 represent mixing ratios among the source waters (Table 3). To separate the effects of mixing ratios changes among and properties of source waters, either mixing ratios or properties were fixed between the 1990s and 2010s. In Case 1, mixing ratios varied with time while the properties of source waters were fixed. For Case 2, mixing ratios were fixed while source water properties changed over time (Table 1, Table 3).

Results

Warming and salinification of AABW in the WSIO

In the WSIO, this study observed that AABW θ increased from -0.41℃ in the 1990s to -0.36℃ in the 2010s over 24.5 years (Δt), indicating a $\Delta\theta$ of +0.05℃ and warming rate (positive $\Delta\theta/\Delta t$) of 0.02 ± 0.01 ^{o}C decade^{-1} (Table 1). Most (> 94%) areas in the AABW domain exhibited significant (95% confidence level) warming between the 1990s and 2010s **(**Fig. 2a, Figure 4a). The observed AABW S_P also increased in the WSIO from 34.660 in the 1990s to 34.664 in the 2010s (Table 1). Therefore, ΔS_P (Δt = 24.5 years) and the rate of S_P increase (positive $\Delta S_P/\Delta t$) was +0.004 and 0.002 ± 0.001 decade^{-1}, respectively (Table 1). Almost everywhere (~100%) within the WSIO AABW domain, significant salinification was found between the 1990s and 2010s (Fig. 2c, Figure 4c)**.**

The warming and salinification of AABW in the WSIO can be explained by changes in θ and S_P with fixed properties of and time-varying mixing ratios among the source waters (Case 1) Figure 3a and Table 1). A reduced (from 66% to 59%) portion of fresh CDBW and increased (from 2% to 6% and 32% to 35%, respectively) portions of warm and saline LCDW

and saline WSDW were mainly responsible for the warming and salinification (Table 3). In contrast, values estimated based on time-varying properties of and fixed mixing ratios among the source waters (Case 2) indicated cooling and freshening trends, contrary to the observations Figure 3a, Table 1). CDBW is the largest contributing source of water to the WSIO AABW, with the highest (59–66%) mixing ratio among the source waters. θ and S_P of CDBW decreased ($\Delta\theta$ = -0.08 ^{o}C and ΔS_P = -0.009) over time (Table 1, Table 3). WSDW also cooled at a rate of 0.01 ± 0.02 ^{o}C decade^{-1} (Table 1, Table 3). Despite LCDW warming and salinification of both WSDW and LCDW, changes in the AABW properties ($\Delta\theta$ and ΔS_P) estimated based on the time-varying properties of fixed mixing ratios among the source waters could not explain the observations (Table 1). Therefore, the warming and salinification of AABW were mainly due to changes in mixing ratios among source waters rather than changes in the source water properties (Figure 3a, Table 1).

Long-term warming and salinification trends in the WSIO AABW have been previously reported (Aoki et al., 2020a; Sallée, 2018). For example, warming and salinification at 0.03 ^{o}C decade^{-1} and < 0.001 decade^{-1}, respectively, between the 1970s and 2010s were found based on observations

in the Enderby Basin (Aoki et al., 2020a) (Figure 1). Slower warming and more rapid salinification between the 1990s and 2010s were observed here compared with those from the more extended period (Table 1). Salinification and overall warming of deep and bottom waters in the northeast Weddell Sea (reported previously as, e.g., ΔS_P of +0.002 between the early 1990s and 2000s (Strass et al., 2020; Fahrbach et al., 2004)) were comparable to the WSDW salinification rate (0.005 decade^{-1}) presented here (Table 1). This WSDW salinification was partly responsible for AABW salinification (Table 3). Warming and salinification of deep and bottom waters in Weddell Sea have been potentially linked to the increasing LCDW flow into AABW beyond the WSDW formation region (Strass et al., 2020). More considerable LCDW inflow into Weddell Sea and resultant salinification of WSDW could be relevant to positive SAM index anomalies over the last decade (Lin et al., 2018), as Ekman suction driven by anomalously strong westerly winds in the SAM positive phase strengthens the Weddell Gyre and ACC, thereby increasing transport of highly saline LCDW into the deep and bottom waters of Weddell Sea (Strass et al., 2020).

Warming and freshening of AABW in the ESIO

As in the WSIO, AABW θ observed along meridional lines in the ESIO also increased from -0.18℃ in the 1990s to -0.13℃ in the 2010s (Δt = 17.0 years), a warming rate (positive $\Delta\theta/\Delta t$) of 0.03 ± 0.01 ^{o}C decade^{-1} (Table 1). In ~96% of the ESIO AABW domain, significant warming was observed between the 1990s and 2010s, similar to that in the WSIO (Fig. 2b and Figure 4b). However, S_P decreased such that the ESIO AABW freshened, from 34.679 in the 1990s to 34.673 in the 2010s; this contrasted with the WSIO salinification (Table 1). Over the 17 years, ΔS_P and $-\Delta S_P/\Delta t$ were -0.006 and 0.004 ± 0.001 decade^{-1}, respectively. Nearly all (~98%) of the ESIO AABW domain experienced significant freshening between the 1990s and 2010s (Fig. 2d and Figure 4d).

The warming and freshening of AABW in the ESIO can be explained by the time-varying properties of and fixed mixing ratios among the source waters (Case 2) that yielded warming and freshening at rates comparable to the observations (Figure 3b and Table 1). S_P decreases between the 1990s and 2010s were significant in all three water sources (LCDW, ALBW, RSBW), and θ increases were found in ALBW and RSBW (Figure 3b and Table 1). In contrast, in Case 1, the observed warming and freshening could

not be reproduced. The mixing ratios of relatively cold and fresh ALBW decreased from 58 to 51%, and those of the warm and saline LCDW slightly increased from 20 to 21%. The ratio of the relatively saline RSBW also increased from 22% to 27% (Table 3). The resulting AABW θ was nearly constant, whereas AABW S_P increased over the study period compared with observations (Figure 3b and Table 1). Thus, the warming and freshening of source waters were responsible for the changes in the ESIO AABW characteristics.

The AABW warming and freshening rates on the west side of the Australian Antarctic Basin (Figure 1) were previously reported as 0.02–0.08 ℃ decade^{-1} and 0.002–0.012 decade^{-1}, respectively (Johnson et al., 2008; Menezes et al., 2017; Purkey and Johnson, 2013; Shimada et al., 2012), comparable to the results in this study (Table 1). The warming and freshening of ESIO AABW are related to the overall warming in Southern Ocean and the freshening of source waters around the Antarctic shelves. Previous studies suggest that bottom waters in the Southern Ocean have warmed at a rate of ~0.05 ºC decade^{-1}, presumably due to increasing ocean heat content (Sallée, 2018); this is consistent with the overall warming of the ESIO AABW in this study (Figure 3b, Table 1). In the ALBW and RSBW

formation regions, near-bottom water saw remarkable decreases in absolute salinity: by 0.05 g kg^{-1} from the late 1960s to the early 2010s and by 0.06 g kg^{-1} from the 1990s to early 2010s (Aoki et al, 2020b). This freshening rate is higher than that of the ESIO AABW detailed here Figure 3b and Table 1. The AABW freshening in Southern Ocean is likely due to increasing sea ice melt, continental ice discharge, and abrupt glacial calving events near the ALBW formation region in 2010 (Aoki et al., 2005; Tamura et al, 2012; Castagno et al., 2019; Jacobs et al., 2002). Such an increase in freshwater input can cause a reduction in dense water formation through brine rejection, resulting in decreases in the AABW volume and salinity (McCartney and Donohue, 2007; Aoki et al., 2020b).

Since the late 2010s, however, salinity has rebounded in the ALBW formation region and western Ross Sea (Aoki et al., 2020b; Castagno et al., 2019). This increase is closely related to the recent (since 2014) increase (~0.07) in the practical salinity of High Salinity Shelf Water (HSSW), a precursor of RSBW (Yoon et al., 2020). Thus, ESIO AABW may have become more saline in the 2020s owing to the continued development of polynya from enhanced katabatic winds (Yoon et al., 2020) and effective sea ice formation rate owing to the unusual combination of positive SAM and

strong El Niño conditions from 2015 to 2018 (Slivano et al., 2020).

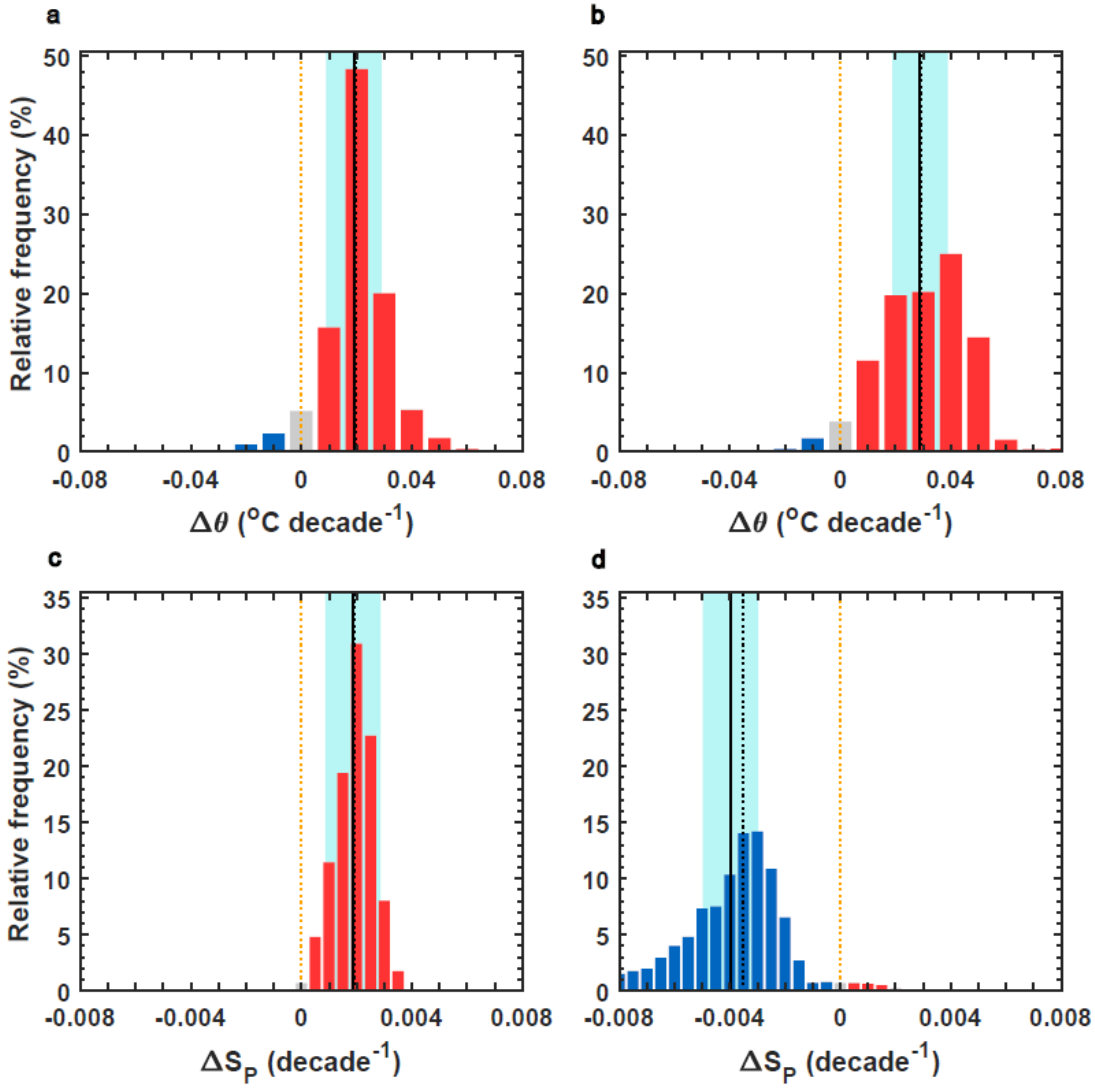

Figure 2. Changes in potential temperature (θ) and practical salinity (S_P) of Antarctic Bottom Water (AABW) in Southern Indian Ocean (SIO). Histograms of $\Delta\theta$ (**a** and **b**) and ΔS_P (**c** and **d**) of AABW in the western SIO (WSIO; **a** and **c**) and eastern SIO (WSIO; **b** and **d**) between the 1990s and 2010s. Blue (red) indicates cooling and freshening (warming and salinification), whereas grey indicates no change. Areas shaded in cyan

represent statistical significance at the 95% confidence interval from the mean, based on Student's *t*-test. The black solid lines indicate mean values, while zero and median values are shown using orange and black vertical dashed lines, respectively.

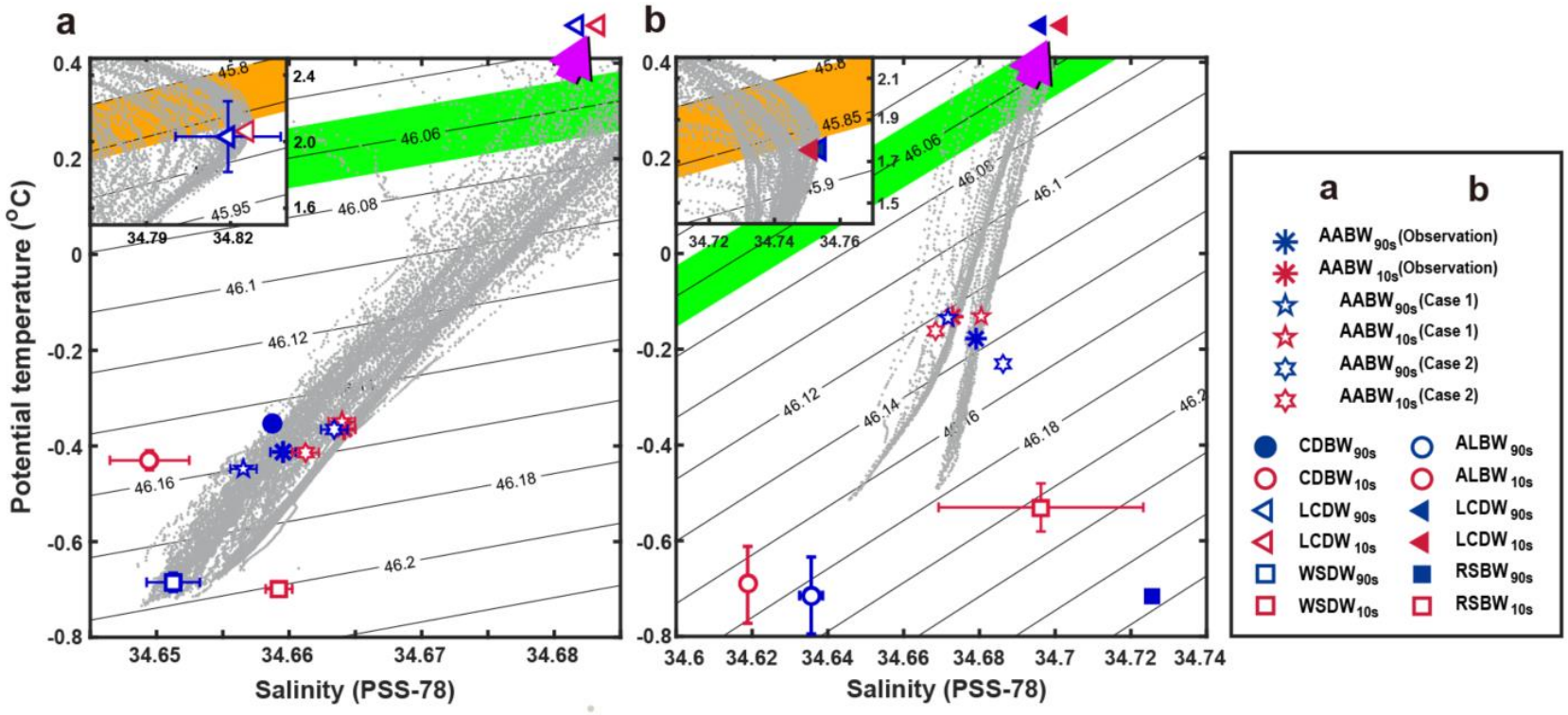

Figure 3. θ-S_P plots of Antarctic Bottom Water (AABW) and source waters in Southern Indian Ocean (SIO).

θ-S_P plots of AABW (marked with asterisks in **a** and **b**) for the 1990s (blue) and 2010s (red) and estimated (Case 1,

five-pointed stars; Case 2, six-pointed stars) in the western SIO (WSIO) (**a**) and eastern SIO (ESIO) (**b**). CDBW (**a**) and ALBW (**b**) are marked with circles, LCDW (**a** and **b**) with triangles, and WSDW (**a**) and RSBW (**b**) with squares. All watermasses are marked with error bars with 95% confidence except filled markers (filled markers are watermasses that cannot estimate their uncertainty due to lack of sample number; see also Table 1). The black contours denote potential density (kg m^{-3}) referenced to 4,000 dbars (σ_4). LCDW properties are found only in the zoomed-out domain (top-left corners) and out of the range in the zoomed-in domain as marked by the purple shaded arrows. Neutral densities of 28.05 and 28.27 kg m^{-3}, corresponding to 45.80– 45.86 kg m^{-3} and 48.05–48.07 kg m^{-3} in σ_4, are shaded in thick orange and green, respectively. Weddell Sea Deep Water, WSDW; Cape Darnley Bottom Water, CDBW; Adélie Land Bottom Water, ALBW; and Ross Sea Bottom Water, RSBW.

Table 3. Ratio (%) with 95% confidence intervals of Case 1 and Case 2. Table shows ratio of AABW composition of source waters in 2010s and 1990s for cases of varying mixing ratios and fixing properties (Case 1) and varying properties and fixing mixing ratios (Case 2) of θ and S_P of source waters in WSIO and ESIO.

			Case 1			Case 2		
WSIO			CDBW	WSDW	LCDW	CDBW	WSDW	LCDW
	Fraction (%)	2010s	59 ± 1	35 ± 1	6 ± 1	58 ± 1	37 ± 1	5 ± 1
		1990s	66 ± 2	32 ± 2	2 ± 1			
ESIO			ALBW	RSBW	LCDW	ALBW	RSBW	LCDW
	Fraction (%)	2010s	51 ± 1	27 ± 1	21 ± 1	51 ± 1	28 ± 1	21 ± 1
		1990s	58 ± 1	22 ± 1	20 ± 1			

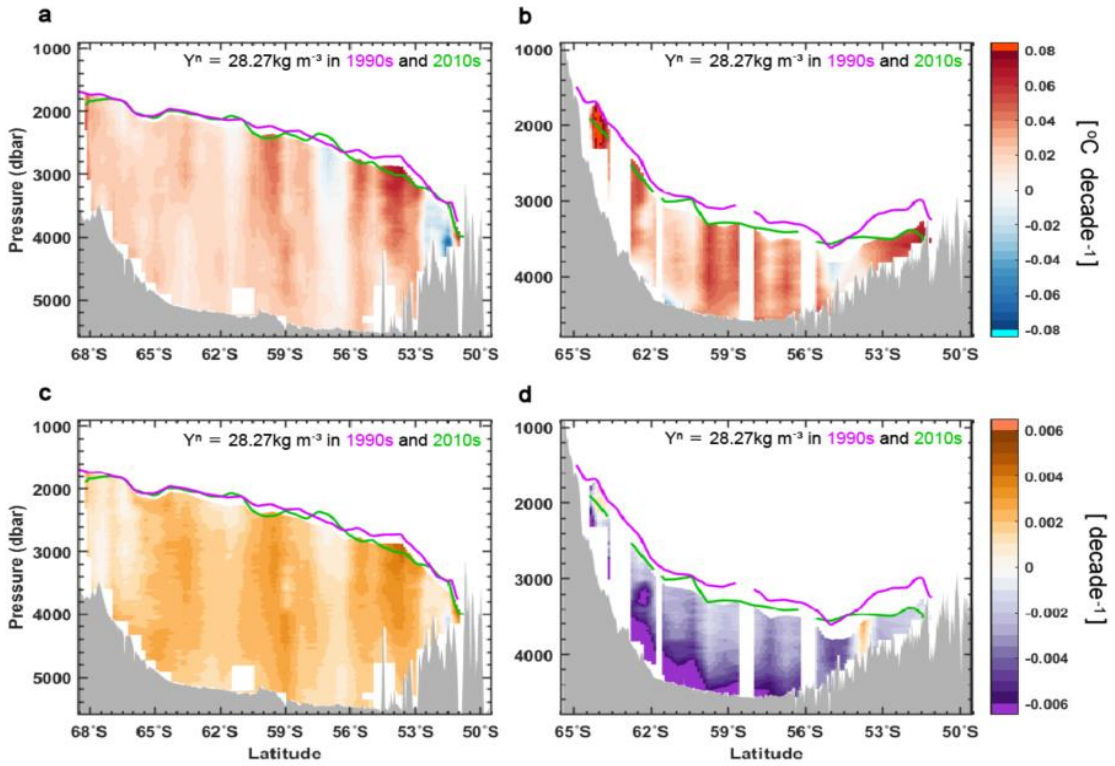

Figure 4. Rates of change in potential temperature and practical salinity. Rates of change in potential temperature (^{o}C decade^{-1}) and salinity (decade^{-1}) in the WSIO (a and c), and ESIO (b and d). Magenta and green lines indicate isopycnals of γ^{n} = 28.27 kg m^{-3} (σ_4; 46.05 - 46.07 kg m^{-3}) in 1990s and 2010s, respectively. Colored domain is defined as the union area where $\theta < 0$ ^{o}C and $\gamma^{n} > 28.27$ kg m^{-3} in whole period of WSIO and ESIO at each.

4. Discussion and conclusions

Implication of contrasting salinity changes in AABW between WSIO and ESIO

A contrasting change in AABW S_P between the WSIO and ESIO (western salinification and eastern freshening) in addition to overall SIO warming over the past three decades was analysed based on changes in the mixing ratio among (Case 1) and properties of (Case 2) source waters. The contrasting salinity changes and overall warming affected the zonal difference in the AABW volume. Consequently, the abyssal circulation was affected, as the AABW upper boundary (e.g., the surface of $\gamma^n = 28.27$ kg m^{-3}) deepened eastward more steeply in the 2010s than in the 1990s, decreasing the AABW volume more so in the ESIO than in the WSIO (Figure 4).

Based on the results, this study assumed that a stronger deep and abyssal flow toward Indian Ocean would have occurred in 2010s due to the different volume changes of the AABW in SIO, and calculated the geostrophic velocity using data from the 1990s and 2010s observed in the zonal section of the SIO (ZSIO) (Figure 1). The AABW structure is divided into a western area (< 80°E) and an eastern area (> 90°E) based on the

Kerguelen Plateau due to the influence of the topography. The isopycnals of neutral density 28.27 kg m^{-3} in the eastern part of the AABW in both areas were deeper than the western part (Figure 5). Also, it was confirmed that γ^n = 28.27 kg m^{-3} isopycnals became deeper in the 2010s than in the 1990s in both areas, i.e. density surface of γ^n = 28.27 kg m^{-3} in the western area of WSIO and ESIO became deeper from 1925 m and 2050 m in 1990s to 1970 m and 2325 m in 2010s, and the eastern area from 3127 m and 2692 m in 1990s to 3159 m and 2865 m in 2010s, respectively (Table 4). It was confirmed that changes in density surface depth lead to a decrease of geostrophic velocity in the eastern area from 0.07 m s^{-1} in the 1990s to 0.06 m s^{-1} in the 2010s, on the other hand, in the western area, it can be seen that there are insignificant changes of geostrophic velocity at 0.05 m s^{-1} in both 1990s and 2010s (Table 4). The intensification of deep and abyssal flow toward Indian Ocean, although still in a reasonable range compared with previous observations (typically few centimetres per second, up to 0.1 m s^{-1}) (Meijers et al., 2010; Aoki et al., 2020a), can substantially impact the deep abyssal circulation and global meridional overturning circulation within and beyond the Indian sector.

The contrasting change in AABW S_P between the WSIO and ESIO

and overall SIO warming also has implications for global sea level rise. Previously estimated steric sea level rises below 3000 dbar were 0.01–0.04 m in the ESIO between the 1990s and 2000s and 0.04–0.07 m between the 1990s and 2010s (Johnson et al., 2008; Menezes et al., 2017). In this study, Sea level changes estimated through the satellite data between 1990s and 2010s were increased 0.04 m in WSIO and 0.06 m in ESIO, and the steric sea level changes for whole water column were estimated almost 0.03 m in WSIO and 0.05 m in ESIO (Table 5).

However, in the case of steric sea level changes relative to 3000 dbar were both increased 0.02 m in SIO, but for different reasons in the east and west (Table 5). This results show most of the sea level changes in the deep and bottom water in the WSIO, but in the ESIO, whole water column contributes to the sea level change (Table 5, Figure 6, Figure 7). Especially, the ratio of AABW below 3000 dbar were 92% and 64% in WSIO and ESIO, respectively. It means that most of the steric sea level rises below 3000 dbar were significantly affected by the AABW. This indicated that east–west contrasts (eastern freshening and western salinification) in the AABW properties between the 1990s and 2010s has significant consequences on steric sea level rise within and beyond SIO.

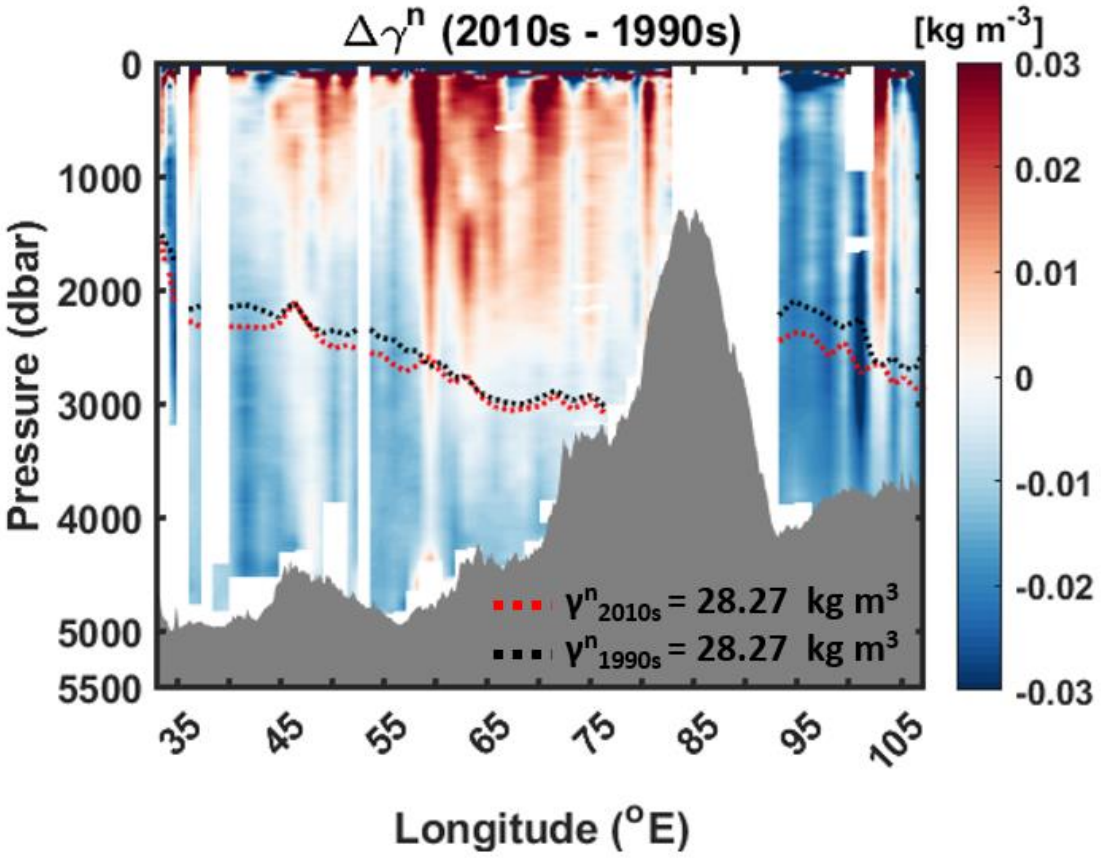

Figure 5. Zonal section of isopycnic surface γ^n = 28.27 kg m^{-3} changes in the SIO between 1990s and 2010s. Zonal section of neutral density anomaly with isopycnic surface γ^n = 28.27 kg m^{-3} changes in the SIO between 1990s (black dashed line) and 2010s (red dashed line) with bottom topography (grey shading area).

Table 4. Depth changes of isopycnals of $\gamma^n = 28.27$ kg m^{-3} in the WSIO and ESIO

Observation Area	Period	D_1* (m)	D_2** (m)	$\triangle D$ ($D_1 - D_2$; m)	$\triangle X$ (distance between D_1 and D_2; m)	Geostrophic velocity (m s^{-1})
WSIO	2010s	1970 ± 10	3159 ± 10	1189 ± 20	2,128,000 ±	0.05 ±
	1990s	1925 ± 12	3127 ± 12	1302 ± 24	2,128,000 ±	0.05 ±
ESIO	2010s	2325 ± 10	2865 ± 10	540 ± 20	713,000 ±	0.06 ±
	1990s	2050 ± 10	2692 ± 10	642 ± 20	713,000 ±	0.07 ±

** Depth of $\gamma^n = 28.27$ kg m^{-3} isopycnals in the western section (WSIO; 33°E, ESIO; 93°E)

** Depth of $\gamma^n = 28.27$ kg m^{-3} isopycnals in the eastern section (WSIO; 77°E, ESIO; 107°E)

Table 5. Total and steric sea level changes observed from satellite altimetry missions and hydrography data between 1990s and 2010.

Variables		Section	
		WSIO	**ESIO**
1. Sea level changes observed from satellite altimetry missions (m)		0.04 ± 0.02	0.06 ± 0.01
2. Steric Sea level changes (whole water column; m)	2_1. Thermosteric effect	0.00 ± 0.02	0.03 ± 0.02
	2_2. Halosteric effect	0.03 ± 0.01	0.02 ± 0.01
	2_3. Thermohalosteric effect	0.03 ± 0.02	0.05 ± 0.02
3. Non-steric sea level changes (1 - 2_3)		0.01 ± 0.02	0.01 ± 0.02
4. Steric Sea level changes (below 3000 dbar)	4_1. Thermosteric effect	0.03 ± 0.01	0.01 ± 0.01
	4_2. Halosteric effect	-0.01 ± 0.01	0.01 ± 0.01
	4_3. Thermohalosteric effect	0.02 ± 0.01	0.02 ± 0.01

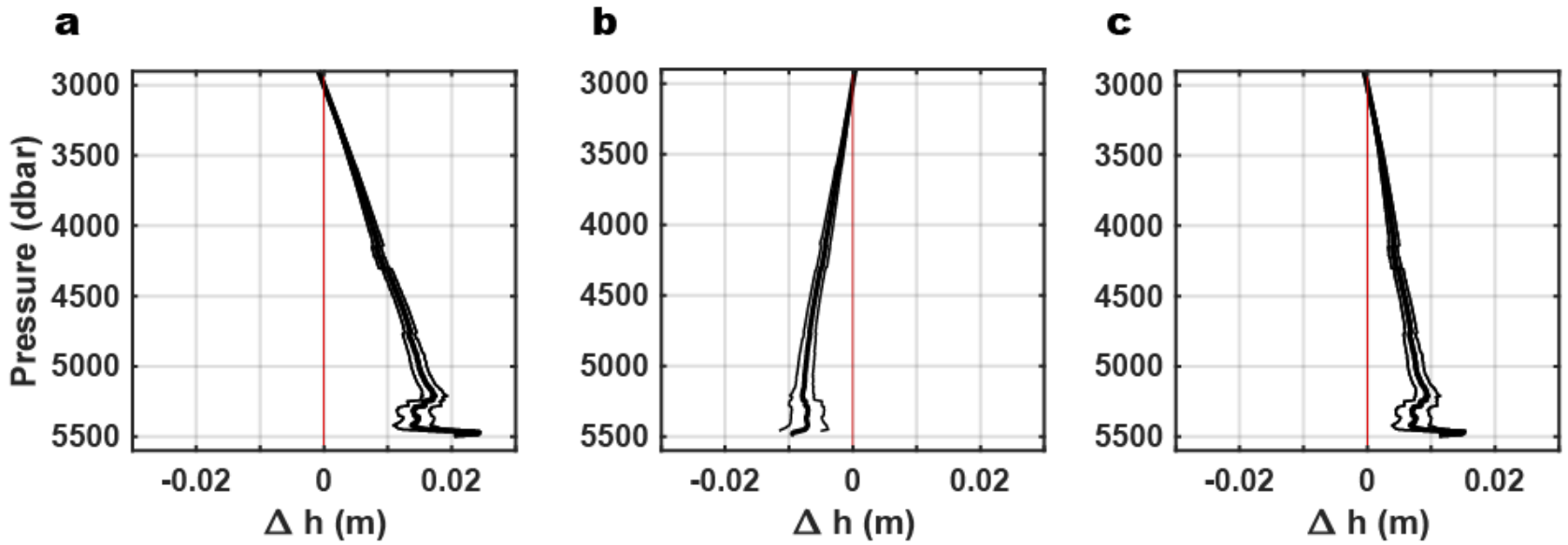

Figure 6. Thermohalo steric sea level changes relative to 3000 dbar between 1990s and 2010s in the WSIO. Steric sea level changes (m) relative to 3000 dbar (black thick lines) with 95% confidence limits (thin black lines) between 1990s and 2010s in the WSIO which consider the impact of temperature (a), salinity (b) and both effects (c).

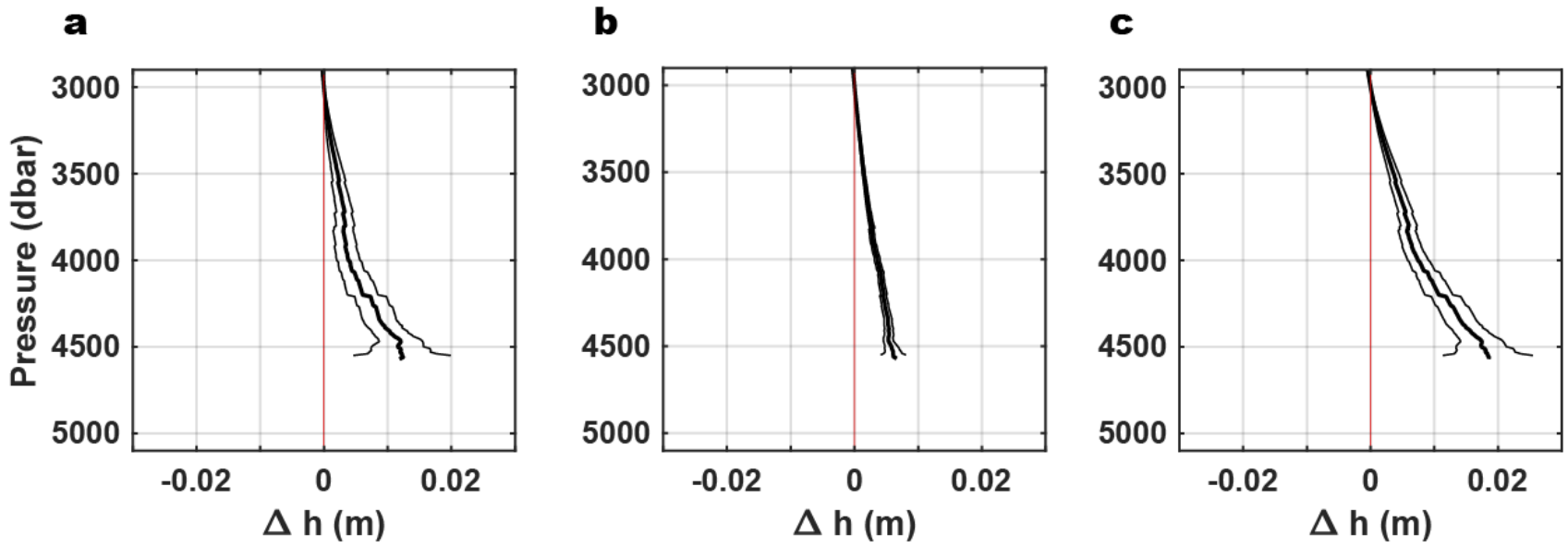

Figure 7. Thermohalo steric sea level changes relative to 3000 dbar between 1990s and 2010s in the ESIO. Steric sea level changes (m) relative to 3000 dbar (black thick lines) with 95% confidence limits (thin black lines) between 1990s and 2010s in the ESIO which consider the impact of temperature (a), salinity (b) and both effects (c).

Acknowledgement

All repeated hydrographic data used in this study are available through the CLIVAR and Carbon Hydrographic Data Office website (https://cchdo.ucsd.edu/). Topography data were provided by the National Oceanic and Atmospheric Administration (NOAA) and Satellite Geodesy at the Scripps Institution of Oceanography, University of California San Diego (https://topex.ucsd.edu/). Sea level changes have been conducted using E.U. Copernicus Marine Service Information (CMEMS). All data needed to draw the conclusions in the paper are present in the paper and/or as supplementary information. Additional data related to this paper may be requested from the authors.

References

Aoki, S. et al. Freshening of Antarctic bottom water off Cape Darnley, East Antarctica. *J Geophys Res* **125**, e2020JC016374 (2020a).

Aoki, S. et al. Reversal of freshening trend of Antarctic Bottom Water in the Australian-Antarctic Basin during 2010s. *Sci Rep* **10**, 14415 (2020b).

Aoki, S., Rintoul, S. R., Ushio, S., Watanabe, S. & Bindoff, N. L. Freshening of the Adélie land bottom water near 140 °E. *Geophys Res Lett* **32**, L23601 (2005).

Cai, W., Shi, G., Cowan, T., Bi, D. & Ribbe, J. The response of the Southern Annular Mode, the East Australian Current, and the southern mid-latitude ocean circulation to global warming. *Geophys Res Lett* **32**, L23706 (2005).

Castagno, P. et al. Rebound of shelf water salinity in the Ross Sea. *Nat Commun* 10, **5441** (2019).

Couldrey, M. P. et al. Remotely induced warming of Antarctic Bottom Water in the eastern Weddell gyre. *Geophys Res Lett* **40**, 2755–2760 (2013).

Fahrbach, E., Hoppema, M., Rohardt, G., Schröder, M. & Wisotzki, A. Decadal-scale variations of water mass properties in the deep Weddell Sea. *Ocean Dyn* **54**, 77–91 (2004).

Jackett, D. R. & McDougall, T. J. A neutral density variable for the world's oceans. *J Phys Oceanogr* **27**, 237-263 (1997).

Jacobs, S. S. & Giulivi, C. F. Large Multidecadal salinity trends near the Pacific–Antarctic Continental Margin. *J Clim* **23**, 4508-4523 (2010).

Jacobs, S. S. Bottom water production and its links with the thermohaline circulation. *Antarct Sci* **16**, 427-437 (2004).

Jacobs, S. S., Giulivi, C. F. & Mele, P. A. Freshening of the Ross Sea during the late 20th century. *Science* **297**, 386–389 (2002).

Johnson, G. C., Purkey S. G. & Bullister J. L. Warming and freshening in the abyssal Southeastern Indian Ocean. *J Climate* **21**, 5351-5363 (2008).

Kusahara, K., Hasumi, H. & Williams, G. D. Impact of the Mertz Glacier Tongue calving on dense water formation and export. *Nat Commun* **2**, 159 (2011b).

Levitus, S., Antonov, J. & Boyer, T. Warming of the world ocean, 1955–2003. *Geophys Res Lett* **32**, L02604 (2005).

Lin, X., Zhai, X., Wang, Z. & Munday, D. R. Mean, variability, and trend of Southern Ocean wind stress: Role of wind fluctuations. *J Climate* **31**, 3557–3573 (2018)

Lumpkin, R.& Speer, K. Global ocean meridional overturning. *J Phys Oceanogr* **37**,2550-2562 (2007).

Mahieu, L. et al. Variability and stability of anthropogenic CO_2 in Antarctic Bottom Water observed in the Indian sector of the Southern Ocean, 1978–2018. *Ocean Sci* **16**, 1559–1576 (2020)

McCartney, M. S & Donohue, K. A. A deep cyclonic gyre in the Australian–Antarctic Basin. *Prog Oceanogr* **5**, 675–750 (2007).

Meijers, A. J. S., Klocker, A., Bindoff, N. L., Williams, G. D. & Marsland, S. J. The circulation and water masses of the Antarctic shelf and continental slope between 30 and 80ºE. *Deep Res Part II Top Stud Oceanogr* **57**, 723-737 (2010).

Menezes, V. V., Macdonald, A. M, & Schatzman C. Accelerated freshening of Antarctic Bottom Water over the last decade in the Southern Indian Ocean. *Sci Adv* **3**, e1601426 (2017).

Ohshima, K. I. et al. Antarctic Bottom Water production by intense sea-ice formation in the Cape Darnley polynya. *Nat Geosci* **6**, 235-240 (2013).

Orsi, A. H. Recycling bottom waters. *Nat Geosci* **3**, 307-309 (2010).

Orsi, A. H., Johnson, G. C. & Bullister, J. L. Circulation, mixing, and production of Antarctic Bottom Water. *Prog Oceanogr* **43**, 55-109 (1999)

Orsi, A. H., Smethie Jr., W. M. & Bullister, J. L. On the total input of Antarctic waters to the deep ocean: A preliminary estimate from chlorofluorocarbon measurements. *J Geophys Res* **107**, C8 (2002).

Purkey S. G. & Johnson, G. C. Antarctic Bottom Water warming and freshening: Contributions to sea level rise, ocean freshwater budgets, and global heat gain. *J Climate* **26**, 6105-6122 (2013).

Purkey, S. G. & Johnson, G. C. Global contraction of Antarctic Bottom Water between the 1980s and 2000s. *J Clim* **25**, 5830–5844 (2012).

Purkey, S. G. & Johnson, G. C. Warming of Global Abyssal and Deep Southern Ocean Waters between the 1990s and 2000s: Contributions to Global Heat and Sea Level Rise Budgets. *J Clim* **23**, 6336-6351 (2010).

Rintoul, S. R. Rapid freshening of Antarctic Bottom Water formed in the Indian and Pacific oceans. *Geophys Res Lett* **34**, L06606 (2007).

Sallée, J.-B. Southern Ocean warming. *Oceanogr* **31**, 52–62 (2018).

Shimada, K., Aoki, S., Ohshima, K. I. & Rintoul, S. R. Influence of Ross Sea Bottom Water changes on the warming and freshening of the Antarctic Bottom Water in the Australian-Antarctic Basin. *Ocean Sci* **8**, 419-432 (2012).

Silvano, A. et al. Recent recovery of Antarctic Bottom Water formation in the Ross Sea driven by climate anomalies. *Nat Geosci* **13**, 780–786 (2020)

Smith, W. H. F. & Sandwell, D. T. Global sea floor topography from satellite altimetry and ship depth soundings. *Science* **277**, 1956-1962 (1997).

Strass, V. H. et al. Multidecadal warming and density loss in the deep Weddell Sea, Antarctica. *J Clim* **33**, 9863–9881 (2020).

Talley, L. D., Pickard, G. L., Emery, W. J. & Swift, J. H. *Descriptive physical oceanography: an introduction* (Academic Press, 2011).

Tamura, T., Williams, G. D., Fraser, A. D. & Ohshima, K. I. Potential regime shift in decreased sea ice production after the Mertz Glacier calving. *Nat Commun* **3**, 1-6 (2012).

Thomas, G., Purkey, S. G., Roemmich, D., Foppert, A. & Rintoul, S. R. Spatial variability of Antarctic Bottom Water in the Australian Antarctic Basin from 2018–2020 captured by deep Argo. *Geophys Res Lett* **47**, e2020GL089467 (2020).

Van Heuven, S. M. A. C., Hoppema, M., Huhn, O., Slagter, H. A. & de Baar, H. J. W. Direct observation of increasing CO_2 in the Weddell Gyre along the Prime Meridian during 1973-2008. *Deep Res Part II Top Stud Oceanogr* **58**, 2613–2635 (2011).

van Wijk, E. M. & Rintoul, S. R. Freshening drives contraction of Antarctic Bottom Water in the Australian Antarctic Basin. *Geophys Res Lett* **41**, 1657–1664 (2014).

Vernet, M. et al. The Weddell Gyre, Southern Ocean: Present knowledge and future challenges. *Rev Geophys* **57**, 623-708 (2019).

Williams, G. D. et al. Antarctic Bottom Water from the Adélie and George V Land coast, East Antarctica (140–149°E). *J Geophys Res* **115**, C04027 (2010).

Yoon, S. T. et al. Variability in high-salinity shelf water production in the Terra Nova Bay polynya, Antarctica. *Ocean Sci* **16**, 373–388 (2020).

Abstract in Korean

최근 30년 남빙양 인도양 구역 남극저층수의 대조적인 동서 염분 변화

최 연
지구환경과학부
서울대학교 대학원

전지구적 대양 컨베이어벨트로 알려진 열염순환/자오면 순환의 핵심 요소 중 하나인 남극저층수(Antarctic Bottom Water; 이하 AABW)는 서로 다른 특성의 몇몇 기원수(source water) 혼합으로 남빙양(남극해)에서 형성된다. 특히 남빙양 인도양 구역의 서부(WEST, 50°S이남, 30°E)와 동부(EAST, 50°S이남, 110-115°E)에서는 AABW가 각각 Cape Darnley Bottom Water (CDBW), Weddell Sea Deep Water (WSDW), Low Circumpolar Deep Water (LCDW)와 Ross Sea Bottom Water (RSBW), Adelie Land Bottom Water (ALBW), LCDW로 구성된다. 본 연구에서는 지난 1990년대와 2010년대에 WEST와

EAST에서 수집된 수심별 수온 및 염분 자료를 이용하여 그 장기 변화를 비교·분석하였으며, 그 원인 규명을 위해 Optimum Multiparameter Analysis 방법을 적용하여 기원수 각각의 특성 변화와 혼합 비율 변화가 관측된 AABW 특성을 얼마나 설명할 수 있는 지 정량적으로 조사하였다. WEST에서 관측된 AABW의 수온과 염분은 지난 20여년간 0.02 ± 0.01 °C decade^{-1}와 0.002 ± 0.001 kg g^{-1} decade^{-1}의 비율로 증가했지만, EAST에서 관측된 AABW는 0.03 ± 0.01 °C decade^{-1}와 -0.004 ± 0.001 kg g^{-1} decade^{-1}의 비율로 수온이 증가하고 염분은 감소했다. WEST에서의 AABW 고온고염화는, 저염의 CDBW 혼합 비율이 66%(1990년대)에서 59%(2010년대)로 감소한 반면, 고염의 WSDW와 고온고염의 LCDW의 혼합 비율은 증가(각각 32%에서 35%, 2%에서 6%로 증가)했기 때문으로 밝혀졌다. 대조적으로 EAST에서의 AABW 고온저염화는 기원수의 혼합 비율보다 기원수 RSBW와 ALBW 자체의 고온저염화(RSBW: 0.08 °C decade^{-1}, -0.013 kg g^{-1} decade^{-1}, ALBW: 0.01 °C decade^{-1}, -0.009 kg g^{-1} decade^{-1})에 따른 것으로 나타났다. 본 연구는 남빙양의 인도양 구역에서 AABW가 전반적으로 온난화되며 동서간의 대조적인 염분

변화(서부 고염화와 동부 저염화)가 나타나는 현상과 그 원인을 최초로 밝혀, 전지구적 열염순환/자오면 순환 장기 변화 이해 및 해수면 변동과 관련해 중요한 시사점을 가진다.

주요 단어: 남극저층수, CTD 반복 관측 데이터, 남빙양 인도양 해역, 지구온난화, 대조적인 염분 변화, 보존 방정식
학 번: 2019-20179

감사의 글

온전한 학위의 길을 끝마치는 단계도 아니면서 감사의 글을 쓰기가 멋쩍지만 그럼에도 석사 과정을 끝맺으면서 인사를 드리고 싶은 분들이 너무 많아지면으로나마 인사 올립니다. 먼저 항상 부족한 제게 가르침을 주신 조양기 교수님, 나한나 교수님께 감사 인사 드립니다. 특히, 어디로 튈지 모르는 공처럼 천방지축인 저를 제자로 받아주시고 갈피를 잡지 못하는 상황 속에서도 굳건히 연구 방향을 잡아주신 제 지도 교수님, 남성현 교수님께 정말 이루 말할 수 없을 만큼 감사하다는 말씀 올립니다. 항상 조언과 격려 아끼지 않고 늘 도움을 주셨던 연구실 선배님들, 윤승태 교수님(그리고 인애 언니), 박재형, 노수연 박사님, 이경재, 이승우, 김형보, 이호준, 김성중 선배님, 그리고 정아, 대홍, 미예 모두 고맙습니다. 또한 물리해양관측연구실과 해양환경예측연구실 선배님 및 구성원 여러분께도 고마움의 인사 전합니다. 무엇보다 길다면 길었을 저의 학위 과정을 애타는 마음에도 불구하고 묵묵하게 기다려주신 저희 어머니를 비롯한 우리 가족들, 최 현, 최재혁, 김재현, 김단우, 김연우, 큰집 식구들, 외가 식구들, 그리고 대학원에서 희로애락을 함께 해준 박유정 박사님, 김건희, 오현경, 김찬미, 그리고 승선 기회와 가르침을 주신 KIOST 및 극지연구소 관계자 여러분 모두 이 자리를 비롯해 감사 인사 올립니다. 그 외에도 언급하지 못했지만 저를 지지하고 응원해주신 제 주변 소중한 분들께도 모두 감사 인사 드립니다. 제 석사 생활에 있어서 앞선 모든 분께서 한 분이라도 계시지 않았다면 제가 학위를 매듭 짓는 순간이 오리란 것을 결코 장담하지 못했을 것입니다. 다시금 고맙습니다. 마지막으로, 그 누구보다 저의 졸업을 바라 마지않고 축하해 주셨을 저의 외조모, 故 김망례 여사님께 이 논문을 바치며 이만 글을 줄이겠습니다. 감사합니다.